KSCE Journal of Civil Engineering (2020) 24(2):377-389
DOI 10.1007/s12205-020-0712-z

pISSN 1226-7988, eISSN 1976-3808
www.springer.com/12205

Geotechnical Engineering

Optimal Location of Piles in Stabilizing Slopes Based on a Simplified Double-Row Piles Model

Changdong Li[a,b], **Wenqiang Chen**[a], **Yingjie Song**[c], **Wenping Gong**[a], **and Qihua Zhao**[b,d]

[a]*Faculty of Engineering, China University of Geosciences, Wuhan 430074, China*
[b]*State Key Laboratory of Geohazard Prevention and Geoenvironment Protection (Chengdu University of Technology), Chengdu 610059, China*
[c]*Dept. of Civil Engineering, Tianjin University, Tianjin 300354, China*
[d]*College of Environment and Civil Engineering, Chengdu University of Technology, Chengdu 610059, China*

ARTICLE HISTORY

Received 19 April 2019
Revised 26 July 2019
Accepted 4 November 2019
Published Online 3 January 2020

KEYWORDS

Slope
Local failure
Double-row stabilizing piles
Optimal location
Limit analysis

ABSTRACT

Embedding single-row piles is often adopted to stabilize slopes in engineering practice. However, for large-scale and complex slopes, single-row piles might not be able to stabilize the slope; rather, double-row piles, even multirow piles, should be adopted. Currently, the optimal locations of double-row stabilizing piles considering local instability of the slope have rarely been studied. In this paper, a simplified analytical model used to analyze double-row pile stabilized slopes is proposed, where the local failure of the slope above the first row of piles is considered. Through the kinematic approach of limit analysis combined with the strength reduction technique, the required resistance forces provided by double-row piles respectively are derived for different pile locations denoted by the rotational angle. Moreover, a framework is developed for analyzing the optimal locations of multirow piles considering multistage potential slip surfaces. The results of an illustrative example are presented, and the reasonableness of the proposed method is verified. It is concluded that the optimal locations of double-row piles lie within middle-lower part of the corresponding stabilized part of the slope. Finally, discussion illustrates the influences of the seismic effects and soil shear strength parameters on the derived optimal pile locations. This study provides novel scientific insight into the optimized design of stabilizing pile locations in engineering practice.

1. Introduction

Slope instability, which results in heavy casualties and huge economic losses every year worldwide (Dai et al., 2002; Tang et al., 2014, 2019), is a significant problem in engineering practice. Engineering measures, which can help either reduce the driving force or increase the resisting force (Ausilio et al., 2001), are often undertaken to stabilize slopes. Stabilizing piles have long been adopted for slope reinforcement (Li et al., 2013; Wu et al., 2017). Various studies regarding the optimal location of single-row piles and the stability of a slope stabilized by the single-row piles have been undertaken (Ito et al., 1981; Chen and Poulos, 1997; Hajiazizi et al., 2017; Li et al., 2017). Nevertheless, single-row stabilizing piles may not be capable of stabilizing large-scale slopes; as such, double-row or even multirow stabilizing piles have been suggested (Shan, 2002; Li et al., 2014; Bozhinova-Haapanen, 2016). For example, Kang et al. (2009) studied the stability of a huge cut slope, which is stabilized through single-row piles in the upper part and double-row piles with the soil nailing in the lower part. Song et al. (2012) investigated the performance of four-row stabilizing piles in a cut slope. Bozhinova-Haapanen (2016) and Shan (2002) also applied double-row and triple-row piles, respectively, for large-scale landslide treatment in transportation engineering. It can be noted that while double-row or multirow stabilizing piles have played a significant role in the reinforcement of large-scale and complex slopes, the issue on the optimal location for double-row or multirow stabilizing piles has rarely been addressed in the literature.

A variety of methods have been developed to examine the optimal location of the single-row stabilizing piles in slopes, which mainly include the limit equilibrium method (Poulos, 1995; Li et al., 2015), the limit analysis method (Qin et al., 2017;

CORRESPONDENCE Qihua Zhao ✉ zhqh@163.com State Key Laboratory of Geohazard Prevention and Geoenvironment Protection (Chengdu University of Technology); College of Environment and Civil Engineering, Chengdu University of Technology, Chengdu 610059, China

Rao et al., 2017) and the numerical method (Chow, 1996; Wei and Cheng, 2009). In addition, many studies have been performed to explore the influence of external factors on the piled slopes, especially the seismic effects (Li et al., 2010; Wang and Zhang, 2013; He et al., 2015), for which different methods, mainly including the pseudostatic method, the stress-deformation method and the permanent-displacement method, have been proposed (Jibson, 2011). Stabilizing piles have been proven to be effective in improving slope stability under frequent seismic activities (Al-Defa and Knappett, 2014; Wang and Zhang, 2014; Ma et al., 2019), and many results of the optimal location of piles in slopes under seismic conditions have been reported in the literature (Li et al., 2016; Li and Yang, 2019). Despite many studies, it is noted that the different methods may yield different optimal locations for the stabilizing piles due to different solutions in tackling the soil-pile interaction effect and the resistance force provided by piles. For example, the results obtained by numerical analysis indicated that the optimal position for stabilizing piles to be installed is in the vicinity of the middle of the slope (Cai and Ugai, 2000; Won et al., 2005); whereas, the results of the limit analysis showed that the optimal piles location is near the slope toe (Li et al., 2006; Li et al., 2012b).

From the abovementioned, the existing studies mainly focus on the stability of single-row piles stabilized slopes and the optimal location of single-row piles. However, as stated previously, it has been suggested that double-row or multirow stabilizing piles are more applicable for the reinforcement of large-scale and complex slopes. Currently, there are only limited studies related to double-row or multirow stabilizing piles applied in large-scale and complex slope reinforcement engineering (Shan, 2002; Kang et al., 2009; Song et al., 2012; Sun et al., 2013; He, 2016). Ito et al. (1982) studied the stabilizing effect of double-row piles and then proposed a design method of multirow stabilizing piles for preventing large landslides. Based on the soil arch theory and limit equilibrium method, Shen et al. (2012) derived the formulas of landslide thrust acting on the front- and rear-row piles of double-row piles. Sun et al. (2013) conducted systematic field monitoring work to investigate the stability of a highway landslide induced by excavation and reinforced by four rows of piles in total. It is noted that most previous studies on double-row or multirow stabilizing piles mainly focused on the reinforcement mechanism and the stability of stabilized slope; few of them have examined the optimal location of double-row or multirow stabilizing piles. Furthermore, almost all of the existing studies focus on the stabilization work for a single slip surface without considering the possible existence of secondary or multistage slip surfaces, whereas some studies (Lei et al., 2006; Liu et al., 2016) and engineering cases (Li et al., 2012a) have reported the occurrence of the local failure of the upper soil sliding out from the top of prearranged single-row stabilizing piles.

This paper presents a study on the optimal locations of double-row piles used for stabilizing unstable slopes. In this study, a simplified analytical model for the double-row pile stabilized slope is proposed, which takes into account the local failure of the upper unstable part of the slope above the first row of piles. The corresponding procedure is put forward for optimizing the locations of double-row piles in the presented simplified analytical model. Based on the proposed analytical model and the corresponding optimization procedure, the kinematic approach of limit analysis combined with the shear strength reduction technique is first introduced for the analysis of the optimal locations of double-row stabilizing piles. Then, the solution for determining the critical slip surface of the slope is derived, and a framework of optimizing multirow pile locations considering multistage slip surfaces is further developed. Thereafter, a case study of a slope example is conducted for illustrating the implementation of the proposed approach. Furthermore, the validation of the proposed simplified analytical model for a double-row pile stabilized slope is carried out. Finally, discussion about the influences of the horizontal seismic coefficient, soil shear strength parameters and other factors on the optimal location of double-row piles is presented. The proposed model and optimization procedure for the locations of double- or multirow stabilizing piles can provide theoretical references for improving the practical design work of piles used for reinforcing unstable slopes.

2. Methodologies

2.1 Shear Strength Reduction Technique

The factor of safety (F_s) of a slope could be defined in a variety of ways, among which three kinds of definitions are generally used (Zheng et al., 2010), including the strength reserve method, the overload factor and the strength reduction method (Bishop, 1955). In this paper, the F_s is exactly adopted as the coefficient of the shear strength reduction that brings the slope to a limit equilibrium state, which is defined as follows (Duncan, 1996; Ausilio et al., 2001; Itasca, 2013):

$$F_s = \frac{c}{c_m} = \frac{\tan\varphi}{\tan\varphi_m} \tag{1}$$

where c and φ are the available cohesion and friction angle of the soil, respectively; c_m and φ_m are the reduced shear strength parameters, respectively, that are required to yield the state of critical stability. The definition shown in Eq. (1) is identical to that adopted in the limit equilibrium methods and has been adopted in many other methods (Michalowski, 1995; Won et al., 2005; Nian et al., 2008).

2.2 The Proposed Simplified Double-Row Pile Stabilized Slope Model

To solve the problem of finding the optimal piles locations for a slope stabilized by double-row piles in the condition of local instability occurs in the upper slope above the first single-row piles (Lei et al., 2006; Liu et al., 2016), a simplified double-row pile stabilized slope model is presented herein, as shown in Fig. 1. The logsprial rotational failure mechanism is adopted in the simplified double-row pile model, which has been found to be

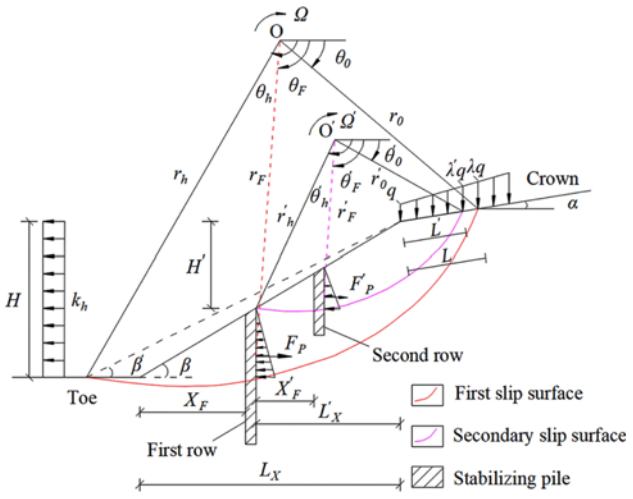

Fig. 1. Rigid Rotation Collapse Mechanism for a Slope Reinforced with Double-Row Piles Considering Local Failure of the Slope

the most adverse slope failure mechanism for a horizontal slope of uniform soil among various slope failure mechanisms (Chen, 1975), and also has been adopted by numerous studies (Michalowski, 1995; Ausilio et al., 2001; Li et al., 2012b). Note that the logspiral failure mechanism assumed in the kinematic approach of limit analysis satisfies not only the equilibrium conditions but also the yield criterion and associated flow rule, which means the logspiral failure mechanism can provide more rigorous solutions but without adding computation complexity than other possible failure mechanisms.

For a potential unstable slope with a log-spiral failure mechanism, as shown in Fig. 1, the geometry of the first slip surface, which refers to the initial slip surface of overall instability of the slope, is described by a log-spiral equation as follows (Ausilio et al., 2001):

$$r_F = r_0 \exp\left[(\theta_F - \theta_0)\frac{\tan\varphi}{F_s}\right] \tag{2}$$

where r_F and r_0 are the corresponding radii of the log-spiral rotational angle θ_F and θ_0, respectively. Similar to the first slip surface, the geometry of the secondary slip surface corresponding to local failure of the soil above the first row of piles is also considered obeying the form of the log-spiral and can be formulated by replacing r_F, r_0, θ_F, θ_0 and F_s in Eq. (2) with r_F', r_0', θ_F', θ_0' and F_S'.

Note that the presented double-row pile model focuses on the problem that the soil above one row of preset stabilizing piles tends to be unstable, such that another row of piles should be installed to stabilize the upper potentially unstable soil body. Thus, it is reasonable to analyze the stabilizing effects of two rows of stabilizing piles respectively in the proposed double-row piles model. Furthermore, the procedure to analyze the optimal location of double-row piles based on the proposed double-row pile model can be summarized as follows:

Step 1: For the predetermined first slip surface (i.e., the initial slip surface) of overall instability, calculate required resistance force provided by the first row of piles under different pile positions; thus, the optimal location for the first row of piles can be determined by acquiring the minimum required resistance force.

Step 2: Considering the possibility for the occurrence of local failure of the soil above the first row of piles, with the assumption that the secondary slip surface slides through the top of the first row of piles, determine the critical secondary slip surface and its factor of safety. Note that while the secondary slip surface is assumed to pass through the top of the piles, the results of an illustrative example and the numerical verification presented later confirm the rationality of this assumption.

Step 3: Judge whether the potential secondary slip surface is safe enough by the obtained safety factor; if not, another row of piles will be needed to stabilize the secondary slip surface. In such conditions, obtain the required resistance force provided by the second row of piles and determine the optimal location for the second row of piles.

2.3 Kinematic Limit Analysis of the Simplified Double-Row Pile Stabilized Slope Model

According to the kinematic theorem of limit analysis, a slope will collapse when the rate of work caused by the external loads and the body forces exceeds the energy dissipation rate for any kinematically admissible failure mode, such as the log-spiral rotational failure mechanism (Fig. 1). Thus, the work-energy balance is the essence of applying the kinematic approach of limit analysis to analyzing pile-stabilized slope problems.

For the proposed double-row pile stabilized slope model (Fig. 1), first, for the analysis of the first row of piles stabilizing the first slip surface, the rate of external work done by the weight of the sliding mass, the vertical linearly distributed surcharge load and the seismic force can be respectively expressed as follows:

$$W_1 = \gamma r_0^3 \Omega (f_1 - f_2 - f_3 - f_4) \tag{3}$$

$$Q = \frac{\lambda+1}{2} qL\Omega\left[r_0\cos\theta_0 - \frac{\lambda+2}{3(\lambda+1)}L\cos\alpha\right] \tag{4}$$

$$W_{qe} = \gamma r_0^3 k_h \Omega (f_5 - f_6 - f_7 - f_8) \tag{5}$$

where γ is the effective unit weight of the soil, Ω is the angular velocity relative to the undefined rotational center point O; q and λq are the overloads acting on the slope shoulder and the sliding-into point of the first slip surface, respectively; k_h is the horizontal seismic coefficient; L is the distance between the sliding-into point of the first slip surface and the slope shoulder (Fig. 1); and $f_1 - f_8$ are functions of α, θ_0, θ_h, φ, β and β', the computations of which are listed in the Appendix (Li et al., 2012b; Nian et al., 2016).

Note that the pseudostatic method (Jibson, 2011; Nian et al., 2016; Xiao et al., 2016) is adopted in this study to incorporate the seismic effects, in which the seismic loading can be represented by the pseudostatic force, which could be captured by a constant horizontal acceleration (a_h) and a constant vertical acceleration (a_v). However, the study by Sarma (1975) noted that the pseudostatic

force in the vertical direction may play a negligible role in evaluating slope stability; therefore, the pseudostatic force in this study is only simulated using the horizontal acceleration $a_h = k_h g$, where g is the gravitational acceleration.

For the computation of the energy dissipation rate of the first stabilized slip surface, note that the sliding mass is dealt as a rigid block and the deformation of the piles is not considered for simplicity in this paper, the energy dissipation occurs both along the slip surface and surrounding the stabilizing piles (Li et al., 2012b). The rate of energy dissipation occurring along the first slip surface can be computed as follows (Li et al., 2012b):

$$D_1 = cr_0^2 \Omega f_9 \tag{6}$$

where the computation of f_9 is given in the Appendix.

To account for the influence of stabilizing piles, a lateral force is assumed to be applied at the pile-soil interfaces; thus, the rate of energy dissipation caused by the first row of stabilizing piles could be expressed as follows (Li et al., 2012b):

$$D_2 = F_p \sin \theta_F r_F \Omega \tag{7}$$

where F_p is the resistance force acting on the unit width of the sliding mass.

In view of the kinematic approach of limit analysis, the slope would be in a state of limit equilibrium when the rate of external work equals the energy dissipation rate; thus, the equation of the work-energy balance of the first stabilized slip surface could be established as follows:

$$W_1 + Q + W_{qe} = D_1 + D_2 \tag{8}$$

Substituting Eqs. (2) – (7) into Eq. (8), the expression of F_p can be obtained as follows:

$$F_p = \frac{\gamma r_0^2 [f_1 - f_2 - f_3 - f_4 + k_h (f_6 - f_7 - f_8 - f_9)] + \frac{\lambda + 1}{2} qL \left[\cos\theta_0 - \frac{(\lambda + 2)}{3(\lambda + 1) r_0} L \cos\alpha \right] - cr_0 f_5}{\sin\theta_F \exp\left[(\theta_F - \theta_0) \frac{\tan\varphi}{F_s} \right]} \tag{9}$$

In Eq. (9), given the geometry of the slope and the designed external load, the safety factor (F_s) of the slope becomes a nonlinear implicit function of F_p, θ_0, θ_h, θ_F and β'. Since the minimum required resistance force (F_p) to achieve the design safety factor is used as the criterion for determining the optimal pile position in this paper (Ausilio et al., 2001; Li et al., 2012b; Nian et al., 2016), only the expression of the required resistance force (F_p) is derived herein.

If the local failure surface is determined with an inadequate safety factor, note that the determination of the critical slip surface will be presented later, then, for the analysis of the second row of piles stabilizing the secondary slip surface, the kinematic approach of limit analysis is also applicable. Due to the assumption that the secondary slip surface passes through the top of the first row of stabilizing piles, the rate of external work caused by the soil weight above the secondary slip surface can be expressed as follows:

$$W_1' = \gamma r_0'^3 \Omega' (f_1' - f_2' - f_3') \tag{10}$$

When the slope is exposed to the vertical linearly distributed surcharge load and the horizontal seismic loading (Fig. 1), the rate of work due to the surcharge load and the seismic loading can be calculated as:

$$Q' = \frac{\lambda' + 1}{2} qL' \Omega' \left[r_0' \cos\theta_0' - \frac{\lambda' + 2}{3(\lambda' + 1)} L' \cos\alpha \right] \tag{11}$$

$$W_{qe}' = \gamma r_0'^3 k_h \Omega' (f_5' - f_6' - f_7') \tag{12}$$

where $\lambda' q$ is the overload acting on the sliding-into point of the secondary slip surface; L' is the distance between the sliding-into point of the secondary slip surface and the slope shoulder (Fig. 1); and the computations of $f_1' - f_3'$ and $f_5' - f_7'$ refer to the computations of the previous $f_1 - f_3$ and $f_5 - f_7$ listed in the Appendix.

Similar to the analysis for the first row of piles, the sliding mass is dealt as a rigid block, and the stabilizing piles are regarded as rigid piles here. The rate of energy dissipation caused by the resistance on the secondary slip surface as well as the pile-soil interfaces can be respectively computed as follows:

$$D_1' = cr_0'^2 \Omega' f_9' \tag{13}$$

$$D_2' = F_p' \sin\theta_F' r_F' \Omega' \tag{14}$$

where the computation of f_9' is similar to the previous f_9 given in the Appendix.

With respect to the kinematic approach of limit analysis, the expression of the required resistance force (F_p') for the second row of stabilizing piles can be obtained as follows:

$$F_p' = \frac{\gamma r_0'^2 [f_1' - f_2' - f_3' + k_h (f_5' - f_6' - f_7')] + \frac{\lambda' + 1}{2} qL' \left[\cos\theta_0' - \frac{(\lambda' + 2)}{3(\lambda' + 1) r_0'} L' \cos\alpha \right] - cr_0' f_9'}{\sin\theta_F' \exp\left[(\theta_F' - \theta_0') \frac{\tan\varphi}{F_s'} \right]} \tag{15}$$

Note that, the proposed expression of the resistance force provided by piles is derived based on the plane strain assumption (Lee et al., 1995; Li et al., 2006; Li et al., 2011). In reality, the pile-soil interaction exists in the horizontal plane for a slope stabilized by a row of discrete piles; however, the rigorous and accurate analytical solution on the pile-soil interaction is still not available in the literature, and thus the pile-soil interaction is out of consideration in the proposed analytical solution in this study, which certainly deserves further studies. Overall, once the critical slip surface is found, then the stabilizing force (F_p or F_p') for the unit width of the sliding mass can be obtained. Furthermore, based on engineering experiences, the pile geometry and center-to-center spacing of piles also can be acquired, then structural requirements can be determined through a pile-soil interaction analysis (Ito et al., 1982; Hassiotis et al., 1997; Li et al., 2019), which is outside the scope of this study.

2.4 Framework of Optimizing the Locations of Multirow Piles Considering Multistage Slip Surfaces

As noted previously, the determination of the critical slip surface is essential for optimizing the piles location. According to the kinematic theorem of limit analysis, the critical slip surface refers to such a slip surface that yields the minimum factor of safety of a slope. Thus, the solution for determining the critical slip surface of a slope based upon a developed optimization program is introduced in this section; further, a framework for optimizing the positions of multirow piles considering multistage slip surfaces is presented.

In reference to the kinematic theorem of limit analysis, for a slope without stabilizing piles, the slope will collapse when the rate of energy caused by the soil weight exceeds the energy dissipation rate due to the resistance along the slip surface; from there, for a given F_s, an upper bound for the slope height could be obtained by equating Eq. (3) to Eq. (6) as follows:

$$H = \frac{\dfrac{c}{2\tan\varphi}\left\{\exp\left[2(\theta_h-\theta_0)\dfrac{\tan\varphi}{F_s}\right]-1\right\}\dfrac{H}{r_0}}{r(f_1-f_2-f_3-f_4)} \tag{16}$$

It can be seen that the H is convertible to the F_s, which is a nonlinear implicit function of θ_0, θ_h and β'; thus, the minimum F_s can be solved by finding the least upper bound for H, and which can be found by minimizing Eq. (16) (Chen, 1975; Ausilio et al., 2001). Obtained θ_0, θ_h and β' define the potential slip surface. Additionally, substituting these angles into Eq. (16) yields the critical height of the slope, which is the maximum height for the slope to remain stable with a specific F_s value. Alternatively, the solution for finding the minimum H could be formulated with the following equations (Ausilio et al., 2001):

$$\begin{cases} \dfrac{\partial H}{\partial \theta_0} = 0 \\ \dfrac{\partial H}{\partial \theta_h} = 0 \\ \dfrac{\partial H}{\partial \beta'} = 0 \\ H = H_{actual} \end{cases} \tag{17}$$

where H_{actual} denotes the actual slope height. In Eq. (17), for an assumed F_s value, the unknown quantities θ_0, θ_h, and β' could be solved through studying the first three partial differential equations. Substituting the obtained angles into Eq. (16), the critical height H can be obtained. When the critical height H equals the actual height H_{actual}, the true safety factor of the slope equals the assumed F_s value.

Nonetheless, in general, it is mathematically difficult to find the values of θ_0, θ_h, and β' by directly solving Eq. (17). Therefore, the solution for Eq. (17) is implemented as a nonlinear constraint optimization problem, which can be set up as follows:

Find: $\theta_0, \theta_h, \beta', F_s$

Subject to: $0 < \theta_0 < \dfrac{\pi}{2}, \theta_0 < \theta_h < \pi, 0 < \beta' \le \beta$ (18)

$H = H_{actual}$

Objective: Minimize $|H - H_{actual}|$

In this paper, an optimization program based on an iterative technique is developed to solve the nonlinear constraint optimization problem. At first, an initial guess for F_s is made to be 1.00, and the shear strength parameters are reduced according to Eq. (1). Next, choose $|H - H_{actual}|$ as the objective and 0.01 degree as the searching increment for θ_0, θ_h, and β', to find critical θ_0, θ_h, and β', when the objective takes its minimum value. Then, judge whether convergence on the objective $|H - H_{actual}|$ is attained for a specified tolerance (e.g., 0.01 m in this paper); if not, adjust the value of F_s and repeat the above process until the tolerance is reached. Thus, the critical slip surface can be located with the derived θ_0, θ_h, and β', and the true safety factor equals the last used F_s.

It is noted that after the first slip surface (i.e., the initial slip surface) of the slope is located, the previously presented procedure for optimizing the locations of double-row piles in section 2.2 can then be performed. Additionally, a third slip

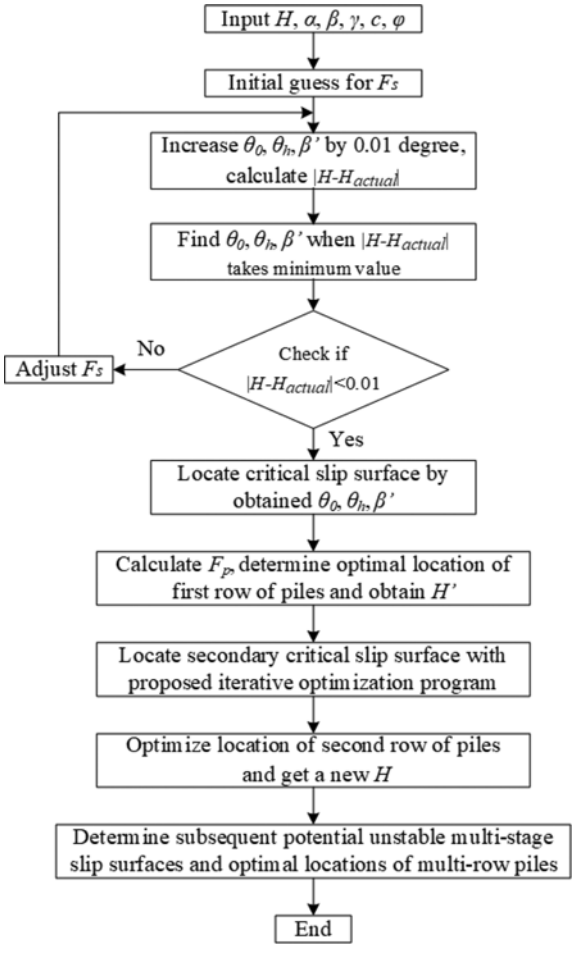

Fig. 2. Solution Flowchart for Multi-Row Piles Location Optimization

surface may be found if local failure of the soil above the second row of piles will probably occur. Therefore, a framework for the optimization of multirow piles locations considering multistage slip surfaces is developed here, of which the detailed flowchart is shown in Fig. 2. In the presented framework, the above optimization program is used to determine the potentially unstable multistage slip surfaces, and the position optimization for the multirow piles is carried out based on the previous procedure for optimizing the locations of double-row piles.

3. Case Study

3.1 Illustrative Example

A homogeneous and dry slope with $H = 13.7$ m and $\beta = 30°$ is analyzed herein as an illustrative example, as shown in Fig. 3. The soil parameters are $c = 18.47$ kPa, $\varphi = 10°$, and $\gamma = 19.63$ kN/m^3. The uniformly distributed vertical surcharge load $q = 20$ kN/m and the horizontal seismic loading, represented by the horizontal seismic coefficient $k_h = 0.025$, are applied to the slope for considering the effects of surcharge load and the seismic loading, respectively. The safety factor of the slope under its natural state is found to be 0.96, which is obviously considered inadequate. A row of stabilizing piles (or possibly double-row of piles if local failure exists) may be installed to improve the slope stability to the design level. Herein, the safety factor of 1.3, which is adopted in some other studies (Ausilio et al., 2001; Li et al., 2012b), is selected as the design safety factor for the illustrative example. According to the proposed kinematic limit analysis approach and the developed optimization framework for pile positions, the optimal design for pile locations is implemented for the slope example.

3.2 Optimal Location of the First Row of Piles

For the slope under three different conditions (i.e., under natural state, with surcharge load and seismic loading separately), the required resistance force F_p provided by the first row of piles to improve slope stability to the design safety factor is plotted against the corresponding rotational angle θ_F (Fig. 4), which denotes the pile position. As can be seen, the required resistance force F_p varies parabolically with increasing rotational angle θ_F in all the cases examined. For example, the relationship between the F_p and θ_F under natural state can be well interpreted by the

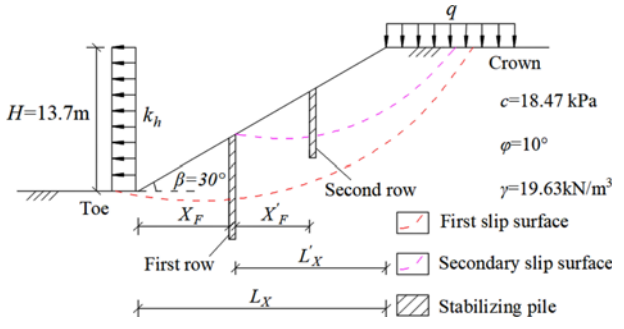

Fig. 3. Illustrative Example of a Slope Reinforced with Double-Row Piles

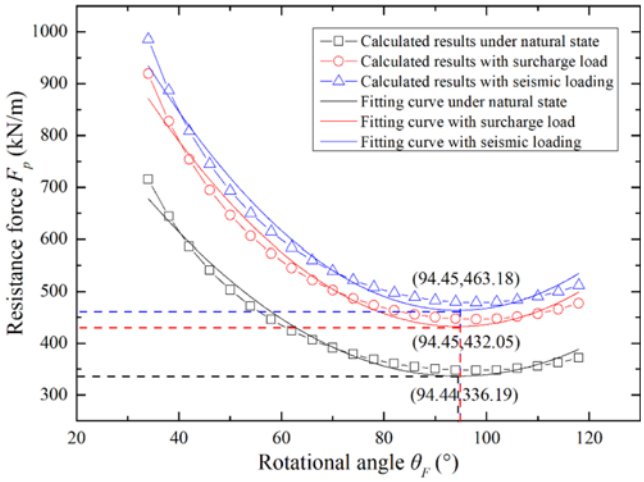

Fig. 4. Curves of Rotational Angle θ_F versus Resistance Force F_p Provided by the First Row of Piles

following equation:

$$F_p = 0.0936 \times \theta_F^2 - 17.6856 \times \theta_F + 1171.3410 \quad (19)$$

More specifically, the F_p decreases first and then increases with increasing θ_F, which means that the position of the piles gradually moves from the slope top to the slope toe. Thus, a minimum value of F_p can be found, and the corresponding rotational angle θ_F can be used to determine the optimal piles location. As illustrated in Fig. 4, both the required F_p with consideration of surcharge load and seismic loading increase compared to those under natural state for the same pile positions, which accords with Eq. (9). It is shown that there is little difference between the optimal pile positions denoted by the rotational angle θ_F in all the cases examined, which are approximately 94.45°, and the corresponding values of X_F/L_X are approximately 0.3848, which implies that the optimal pile positions lie within the middle-lower part of the slope.

3.3 Optimal Location of the Second Row of Piles

For the slope example stabilized by single-row piles installed at the optimal location obtained in the previous section, based upon the proposed solution for finding critical slip surface, the upper slope above the single-row piles is found to possess a potential slip surface with a safety factor of 1.27, which is also regarded as inadequate compared to the design safety factor of 1.30. Thus, another row of piles is necessary for stabilizing the potential secondary slip surface.

As depicted in Fig. 5(a), a similar changing trend as that shown in Fig. 4, can be seen in the required resistance force F_p', whereas it is observed that compared with the first row of piles, the relationship between the required resistance force under surcharge load and that under seismic loading is opposite. The inverse relation indicates that the effect of the seismic loading on the required resistance force is influenced more by the volume of the unstable soil body than is the effect of the surcharge load, which accords with Eqs. (11) and (12). Additionally, the F_p' value is

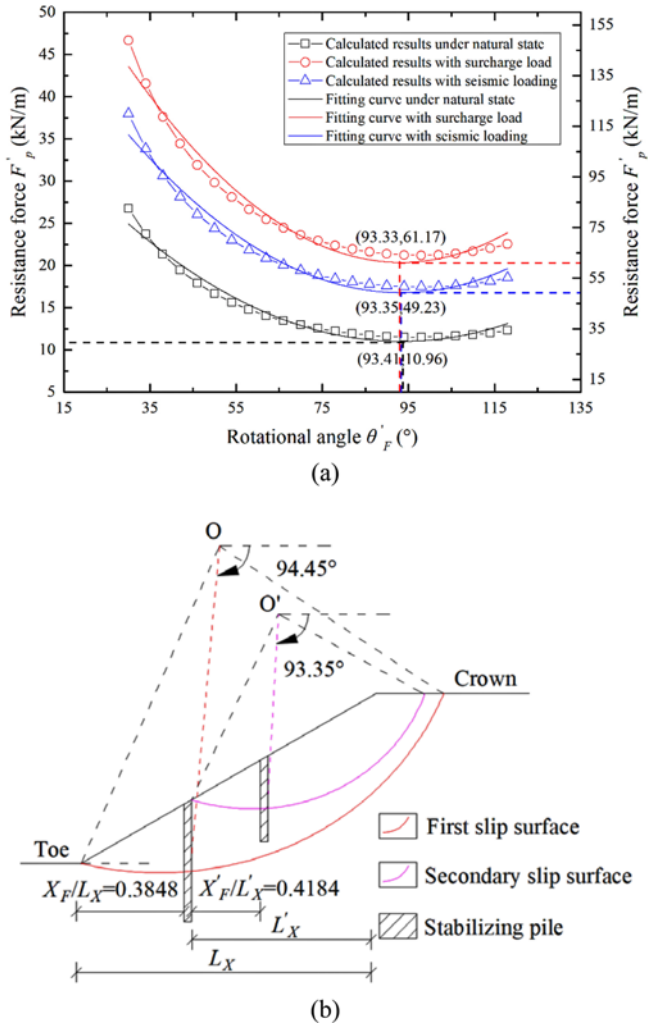

Fig. 5. Results for the Optimization of Piles Location for the Second Row of Piles: (a) Curves of Rotational Angle θ_F' versus Resistance Force F_p' Provided by the Second Row of Piles, (b) Sketch of the Optimal Locations for Double-Row Piles

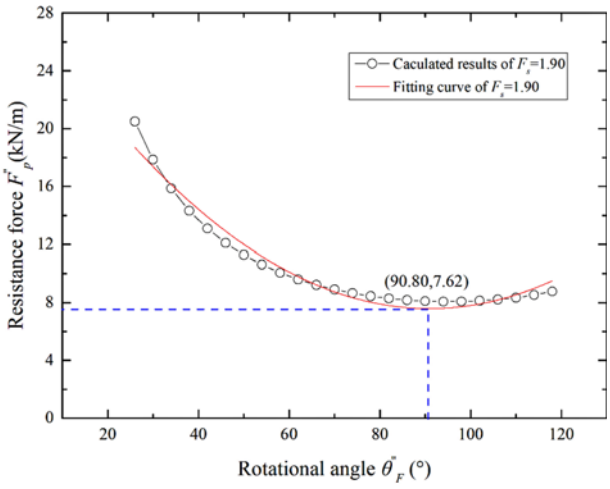

Fig. 6. Curves of Rotational Angle θ_F'' versus Resistance Force F_p'' Provided by the Third Row of Piles for Required Safety Factor of 1.90

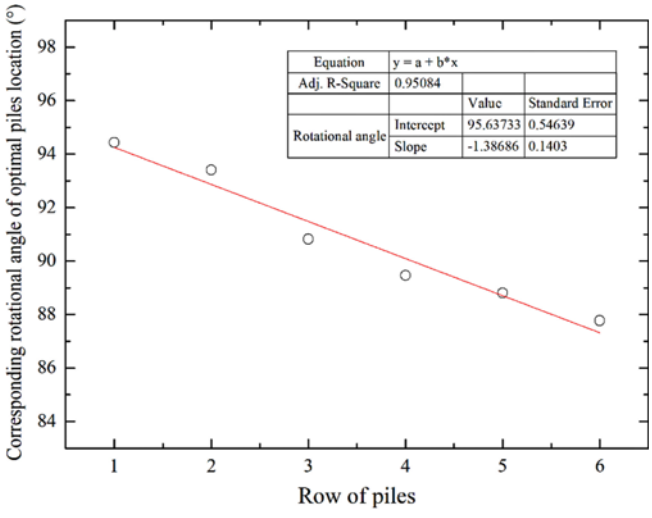

Fig. 7. Relationship between Corresponding Rotational Angle of Optimal Piles Location and the Row of Stabilizing Piles

smaller than the F_p value shown in Fig. 4 under the same conditions, which can be ascribed to the decrease in the volume and the increase in the safety factor of the secondary potential unstable soil body. Furthermore, the optimal pile positions for the second row of piles determined by the rotational angle θ_F' are found to be close to 93.35° under three conditions, which are smaller than that of the first row of piles; and the corresponding X_F'/L_X' are approximately 0.4184, indicating that the optimal positions of the second row of piles are in the middle-lower part of the secondary slip surface. A sketch of the obtained optimal locations for the double-row piles proposed in this paper is presented in Fig. 5(b).

3.4 Arrangement Scheme for the Multirow Stabilizing Piles

As indicated in the previous results, the rotational angle of the second row of piles, which denotes the optimal location, decreased compared with that of the first row of piles. To further investigate the relationship between the optimal pile locations and the row of stabilizing piles, the location optimization for the subsequent multi rows of piles under natural state is implemented based upon the proposed framework in section 2.4, assuming that the subsequent multistage potential slip surfaces are not adequate in the safety requirement. For instance, a third potential slip surface under natural state is determined for the soil mass above the second row of piles with a safety factor of 1.81. Subsequently, the optimal position of the third row of piles is determined to be 90.80° for the required safety factor of 1.90 (Fig. 6), and the corresponding X_F''/L_X'' is 0.4822. The curve of the corresponding rotational angle denoting the optimal pile locations versus the row of piles is plotted in Fig. 7. It can be clearly observed that there exists a strong negative linear relationship between the optimal rotational angle and the row of stabilizing piles, which implies that the optimal locations of multirow piles gradually move toward the slope top from the middle-lower part of the corresponding multistage slip surfaces. For illustrative purposes, a

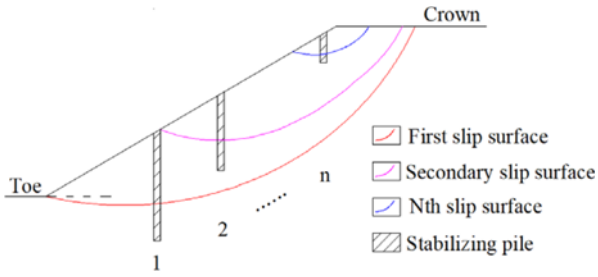

Fig. 8. Sketch of Arrangement for Multi-Row Stabilizing Piles

sketch for the arrangement of multirow stabilizing piles is provided in Fig. 8 for the case where the multirow piles are required to stabilize a slope with a multistage local failure mode.

4. Validation of the Proposed Simplified Double-Row Piles Stabilized Slope Model

A typical slope example previously examined by Ausilio et al. (2001) and Li et al. (2012b) is herein illustrated to verify the reasonableness of the proposed solution for pile-stabilized slopes. The typical slope has the same geometry as the illustrative example shown in Fig. 3, while its shear strength parameters are different, which are $c = 23.94$ kPa and $\varphi = 10°$. With the proposed methodology in this paper, the relationship between the required resistance force F_p and the pile position denoted by the dimensionless abscissa X_F/L_X, namely the ratio between the distance of the pile location to the slope toe and that of the slope toe to the edge of the slope, is obtained for this typical slope under natural state, as shown in Fig. 9. Obviously, the result derived in this paper is slightly lower than that derived in Li et al. (2012b), whereas the obtained required resistance force in this paper varies with the distance ratio X_F/L_X in a similar way as that presented in Li et al. (2012b). The slight difference between the two lines in Fig. 9 may be attributed to the fact that the Ito-Matsui plasticity theory, which takes into account the pile-soil interaction, was adopted to determine the F_p in Li et al. (2012b); however, the pile-soil interaction is not considered in this paper for simplicity as it is not the focus of the study. Despite the slight difference, it should be noted that the optimal pile locations determined by the result in this paper, where the optimal X_F/L_X is approximately equal to 0.4, are also located between the middle and the toe of the typical slope, which is in agreement with the previous study (Li et al., 2012b).

To further verify the rationality of the aforementioned solution for the critical slip surface and the assumption that the slip surface of local failure slides through the top of the front row of stabilizing piles, the shear strength reduction method (SRM) via FLAC^{3D} finite difference software is applied to conduct stability analysis of the slope example in section 3.1. The slope model used in the finite difference analysis has the same geometry and soil parameters as the slope example analyzed in section 3.1. The distances from the left boundary to the slope toe and the right boundary to the slope shoulder are both 24 m, approximately

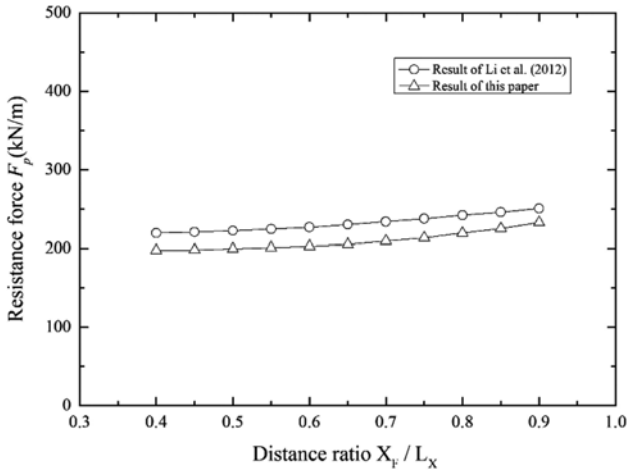

Fig. 9. Results Comparison of Li et al. (2012b) and This Paper for the Typical Slope

Table 1. Constitutive Model and Material Properties Adopted in the Numerical Analysis

Materials	Constitutive model	Material properties
Soil	Linear elastic-perfectly plastic model	$\gamma = 19.63$ kN/m^3, $c = 18.47$ kPa, $\varphi = 10°$ $E = 100$ MPa, $\upsilon = 0.30$
Pile	Linear elastic model	$E = 100$ GPa, $\upsilon = 0.20$ $K_n = 10$ GPa, $K_s = 10$ GPa

equivalent to the horizontal length of the slope. A distance of 20 m is considered between the bottom boundary and the slope bottom. To better validate the results of theoretical analysis in a plane strain mode (Chen and Martin, 2002; Ellis et al., 2010; Li et al., 2011), the model is established with one unit thickness (1 m) and restrained in the lateral direction. Modelled using the pile element, two stabilizing piles with a diameter of 0.8 m are successively arranged along the central section of the model to investigate the response of double-row piles stabilized slope. The maximum size of the element of grid of 0.5 m is adopted for the finite difference mesh division, because of the steady results in terms of stability and critical slip surface through a set of preliminary simulations. The final mesh of the numerical model is constituted by 16896 hexahedral zones. The constitutive model and material properties for the soil and pile are tabulated in Table 1. After the slope model is first set up with applied boundary conditions and material properties, the initial stress state is calculated by bringing the slope model into initial equilibrium state under gravity loading. Then, the stabilizing piles are installed successively according to the obtained theoretical results in this paper. At last, the stability analysis of the slope model is performed based on SRM implemented in FLAC^{3D}.

Through numerical calculation by SRM in FLAC^{3D}, the critical slip surface can be determined by the contour of maximum shear strain increment (Cheng et al., 2007; Pandit et al., 2018; Zhang et al., 2018). The comparison between the theoretical analysis and numerical results of the critical slip surface has been made, as shown in Fig. 10. Apparently, it can be noted that the

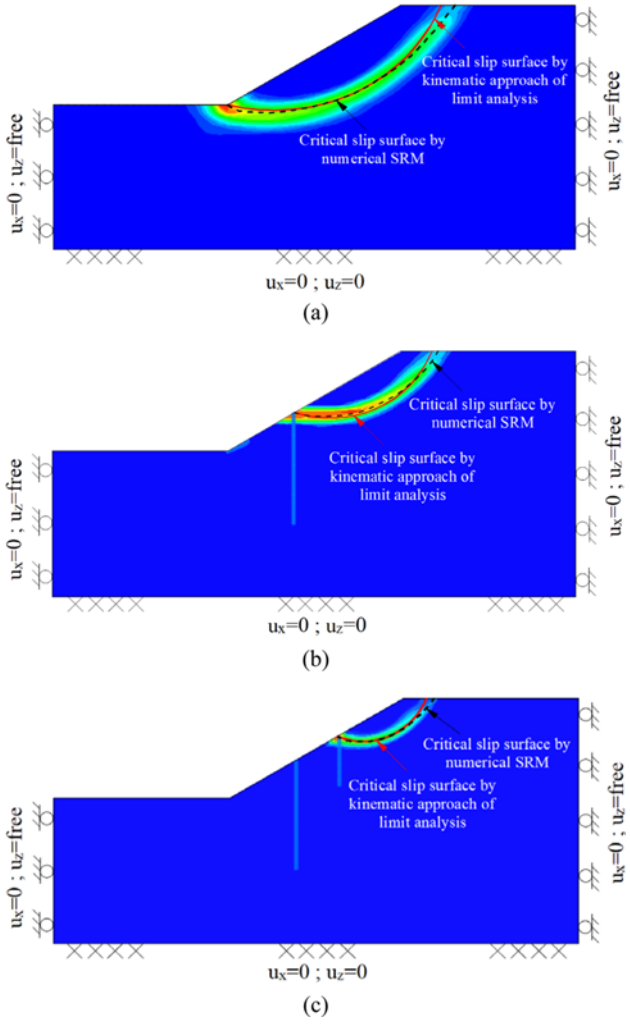

Fig. 10. Comparisons of Critical Slip Surfaces Determined by Kinematic Approach of Limit Analysis and Numerical SRM: (a) Illustrative Example without Reinforcement, (b) Illustrative Example Stabilized by Single-Row Piles, (c) Illustrative Example Stabilized by Double-Row Piles

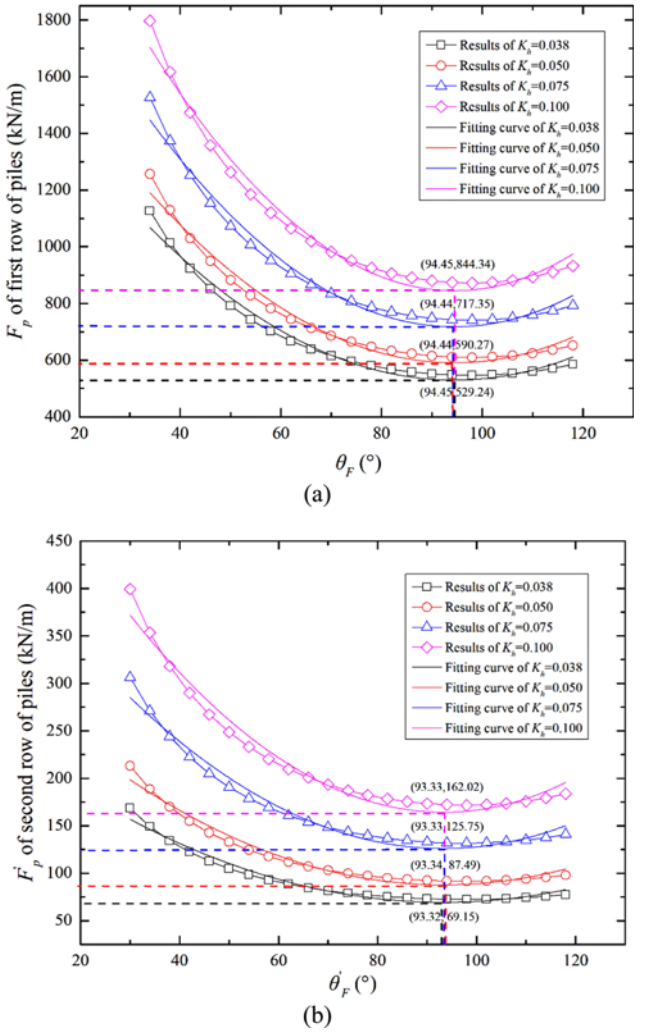

Fig. 11. Curves of Rotational Angle θ_F (θ_F') against Resistance Force F_p (F'_p) under Different Horizontal Seismic Coefficient k_h: (a) The First Row of Stabilizing Piles, (b) The Second Row of Stabilizing Piles

obtained results of the first, secondary and third critical slip surfaces with two different methods are consistent with each other, which fully demonstrates the reasonableness of the assumption about the slip surface of local failure. In addition, safety factors of the slope example before and after reinforcement with the first and second row of piles are also obtained, which are 0.97, 1.33 and 1.86, respectively. Compared with theoretical results of 0.96, 1.27 and 1.81, the numerical results are slightly larger but relative errors between them are still small (no more than 4%), which proves the correctness and rationality of the proposed solution more sufficiently.

5. Discussions

5.1 Influence of the Horizontal Seismic Coefficient on the Optimal Location of Piles

To better illustrate the effect of seismic loading on the optimal locations of double-row piles, the relationship between the resistance force provided by double-row piles under seismic loading and the different horizontal seismic coefficients k_h is plotted in Fig. 11. As can be seen, a larger resistance force is required when the horizontal seismic coefficient k_h increases; the required resistance force provided by the second row of piles is also lower than that of the first row of piles in all the cases examined. Moreover, for either the first row or the second row of piles, the obtained corresponding rotational angles of the optimal pile locations are almost the same under different horizontal seismic coefficients k_h, which suggests that seismic loading may have little effect on the optimal locations of double-row piles.

5.2 Influences of Soil Shear Strength Parameters on the Optimal Location of Piles

To investigate the impact of the variability of soil parameters on the optimal location of piles, another homogeneous and dry slope with $H = 13.7$ m and $\beta = 30°$ has been analyzed, and its soil

properties are c = 12.84 kPa, φ = 10°, and γ = 19.63 kN/m^3. The results of the optimal locations varying with the shear strength parameters of the soil are shown in Fig. 12 for double-row stabilizing piles under natural state. It can be concluded from Fig. 12 that the internal friction angle and the cohesion have inverse effects on the optimal locations of double-row stabilizing piles. More specifically, the optimal piles location gradually moves closer to the outlet of each corresponding failure surface with the increase in the internal friction angle, indicated by the increasing rotational angle, whereas the first decreasing and then stable rotational angle accompanied with increasing cohesion suggests the optimal pile location moving closer to the slope top first and remaining approximately constant later. Moreover, it's also found that the corresponding rotational angle of the optimal pile location for the second row is smaller than that for the first row of piles, which is consistent with the previous results.

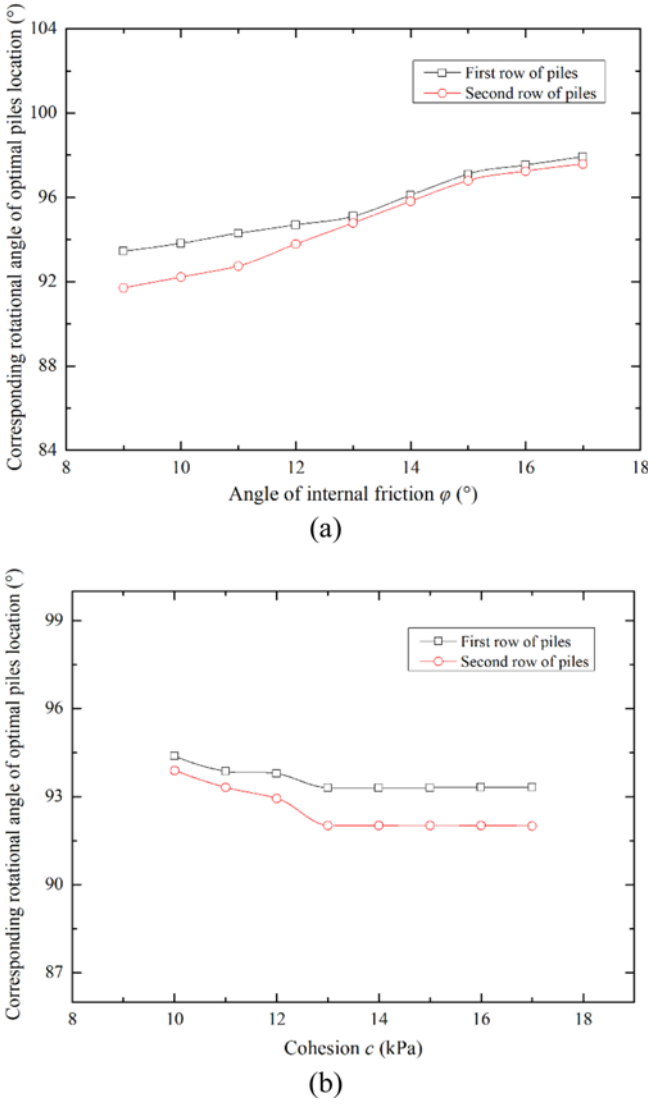

Fig. 12. Effects of Soil Shear Strength Parameters on the Corresponding Rotational Angle of Optimal Location of Piles: (a) The Internal Friction Angle of Soil, (b) The Cohesion of Soil

5.3 Other Factors Affecting the Optimal Pile Locations

It should be noted that significant simplification regarding the pile resistances has been made in this study for deriving the optimal locations of double-row stabilizing piles. As the conventional kinematic approach of limit analysis regards the reinforcement effect provided by the piles as an additional shearing resistance along the potential slip surface, a lateral effective stabilizing force is assumed to be applied at the pile-soil interfaces in this paper to take into account the effect of the stabilizing piles. Therefore, the exact components of the lateral effective stabilizing force, such as the soil resistance before the stabilizing piles, have been considered comprehensively but not reflected separately in this study, which is worthy of further studies.

Additionally, the influence of the groundwater on the stability of the piled slope and the optimal pile locations is not considered in this paper. The homogeneous soil condition is also assumed in the proposed analytical model. The inhomogeneous and anisotropic properties of the soil and slopes with multilayer soils certainly deserve more in-depth future researches. Furthermore, the construction costs and protected objects are not taken into account when searching for the optimal pile location in this study. It should be noted that, in engineering practice of slope reinforcement, the arrangement of stabilizing piles must be combined with concerns on the construction costs and the distribution condition of the protected objects such as highway, railway, residential area and so on.

6. Conclusions

This paper presents a simplified double-row pile stabilized slope model, based on which a procedure is put forward for the analysis of the optimal locations of double-row piles. Different from previous studies, the kinematic approach of limit analysis combined with the shear strength reduction technique is proposed to derive the optimal pile locations under different conditions from the perspective of the optimal rotational angle. Furthermore, a framework for determining the optimal locations of multirow stabilizing piles is developed. Through comparisons with the existing results and numerical results via SRM, the rationality and reasonableness of the proposed analytical solution for the presented double-row pile stabilized slope model are verified.

The proposed procedure for deriving the optimal locations of double-row piles is expounded by illustrating a slope example. The results show that seismic loading and surcharge load both have significant effects on increasing the required resistance force provided by the stabilizing piles, specifically indicating that the effect of seismic loading is more dependent on the volume of the unstable soil body than on the surcharge load. Moreover, the obtained optimal locations of double-row piles for the illustrative slope example under different conditions are approximately 94.45° for the first row and 93.35° for the second row, which suggests that the optimal locations for double-row piles lie within the middle-lower part of the corresponding failure part of the slope.

The developed framework for determining the optimal locations of multirow stabilizing piles is further demonstrated with the illustrative example. The results imply that the corresponding rotational angles of the optimal locations of multirow piles decrease approximately linearly with the row of piles, which indicates that the optimal locations of multirow piles gradually move toward the slope top from the middle-lower part of the corresponding multistage slip surfaces.

In addition, parametric study shows that seismic loading has little influence on the optimal locations of double-row piles, whereas the optimal locations of double-row piles move toward the outlet of each corresponding failure surface with the increase in the internal friction angle while moving toward the slope top at the beginning and remaining approximately constant later with increasing cohesion of the soil. The present paper provides a solution for determining the optimal locations of double-row and even multirow stabilizing piles in a slope with local failure surfaces, which helps improve the practical design procedure of stabilizing piles to some extent. Note that the influences of factors such as groundwater, soil properties of heterogeneity and anisotropy and complex slope geometry are not considered herein, which certainly deserve in-depth future studies.

Acknowledgements

This research is supported by the National Key R&D Program of China (grant nos. 2017YFC1501304 and 2018YFC1507200), the National Natural Science Fund of China (grant nos. 41922055, 41931295, 41630643 and 41702294), the Open Fund of State Key Laboratory of Geohazard Prevention and Geoenviroment Protection (grant no. SKLGP2017K017) and the Fundamental Research Funds for the Central Universities, China University of Geosciences (Wuhan) (grant no. CUGCJ1701).

ORCID

Changdong Li https://orcid.org/0000-0001-7902-7828
Wenqiang Chen https://orcid.org/0000-0001-8269-5480
Yingjie Song https://orcid.org/0000-0001-6958-2959
Wenping Gong https://orcid.org/0000-0003-3062-313X
Qihua Zhao https://orcid.org/0000-0002-6251-4168

References

Al-Defa AH, Knappett JA (2014) Centrifuge modeling of the seismic performance of pile-reinforced slopes. *Journal of Geotechnical and Geoenvironmental Engineering* 140(6):04014014, DOI: 10.1061/(ASCE)GT.1943-5606.0001105

Ausilio E, Conte E, Dente G (2001) Stability analysis of slopes reinforced with piles. *Computers and Geotechnics* 28(8):591-611, DOI: 10.1016/s0266-352x(01)00013-1

Bishop AW (1955) The use of slip circle in the stability analysis of earth slopes. *Géotechique* 5(1):7-17, DOI: 10.1680/geot.1955.5.1.7

Bozhinova-Haapanen A (2016) Stabilizing the landslide on Road E87 Burgas – MalkoTarnovo, Bulgaria. *Procedia Engineering* 143:650-657, DOI: 10.1016/j.proeng.2016.06.092

Cai F, Ugai K (2000) Numerical analysis of the stability of a slope reinforced with piles. *Soils and Foundations* 40(1):73-84, DOI: 10.3208/sandf.40.73

Chen WF (1975) Limit analysis and soil plasticity. Elsevier Science Press, Amsterdam, Netherlands, DOI: 10.1016/b978-0-444-41249-2.x5001-x

Chen CY, Martin GR (2002) Soil-structure interaction for landslide stabilizing piles. *Computers and Geotechnics* 29(5):363-386, DOI: 10.1016/s0266-352x(01)00035-0

Chen LT, Poulos HG (1997) Piles subjected to lateral soil movements. *Journal of Geotechnical & Geoenvironmental Engineering* 123(9):802-811, DOI: 10.1061/(asce)1090-0241(1997)123:9(802)

Cheng YM, Lansivaara T, Wei WB (2007) Two-dimensional slope stability analysis by limit equilibrium and strength reduction methods. *Computers and Geotechnics* 34(3):137-150, DOI: 10.1016/j.compgeo.2006.10.011

Chow YK (1996) Analysis of piles used for slope stabilization. *International Journal for Numerical and Analytical Methods in Geomechanics* 20(9):635-646, DOI: 10.1002(sici)1096-9853(199609)20:9<635::aid-nag839>3.3.co;2-o

Dai FC, Lee CF, Ngai YY (2002) Landslide risk assessment and management: An overview. *Engineering Geology* 64(1):65-87, DOI: 10.1016/s0013-7952(01)00093-x

Duncan JM (1996) Limit equilibrium and finite element analysis of slopes. *Journal of Geotechnical Engineering* 122(7):577-596, DOI: 10.1061/(asce)0733-9410(1996)122:7(577)

Ellis EA, Durrani IK, Reddish DJ (2010) Numerical modelling of discrete pile rows for slope stability and generic guidance for design. *Geotechnique* 60(3):185-195, DOI: 10.1680/geot.7.00090

Hajiazizi M, Bavali M, Fakhimi A (2017) Numerical and experimental study of the optimal location of concrete piles in a saturated sandy slope. *International Journal of Civil Engineering* 16(10):1293-1301, DOI: 10.1007/s40999-017-0155-1

Hassiotis S, Chameau JL, Gunaratne M (1997) Design method for stabilization of slopes with piles. *Journal of Geotechnical and Geoenvironmental Engineering* 123(4):314-323, DOI: 10.1061/(asce)1090-0241(1997)123:4(314)

He J (2016) An optimized design method of treatment for landslides under stepped overloaded plants. *Chinese Journal of Rock Mechanics and Engineering* 35(4):837-846, DOI: 10.13722/j.cnki.jrme.2015.0786 (in Chinese)

He Y, Hazarika H, Yasufuku N, Han Z, Li YG (2015) Three-dimensional limit analysis of seismic displacement of slope reinforced with piles. *Soil Dynamics and Earthquake Engineering* 77:446-452, DOI: 10.1016/j.soildyn.2015.06.015

Itasca (2013) Fast lagrangian analysis of continua, theory and background, factor of safety. Itasca Consulting Group, Inc., Minneapolis, MN, USA, 1-11

Ito T, Matsui T, Hong WP (1981) Design method for stabilizing piles against landslide — One row of piles. *Soils & Foundations* 21(1):21-37, DOI: 10.3208/sandf1972.21.21

Ito T, Matsui T, Hong WP (1982) Extended design method for multi-row stabilizing piles against landslide. *Soils & Foundations* 22(1):1-13, DOI: 10.3208/sandf1972.22.1

Jibson RW (2011) Methods for assessing the stability of slopes during earthquakes — A retrospective. *Engineering Geology* 122(1-2):43-50, DOI: 10.1016/j.enggeo.2010.09.017

Kang GC, Song YS, Kim TH (2009) Behavior and stability of a large-

scale cut slope considering reinforcement stages. *Landslides* 6(3):263-272, DOI: 10.1007/s10346-009-0164-5

Lee CY, Hull TS, Poulos HG (1995) Simplified pile-slope stability analysis. *Computers & Geotechnics* 17(1):1-16, DOI: 10.1016/0266-352x(95)91300-s

Lei WJ, Zheng YR, Feng XT (2006) Analysis of pile location on landslide control. *Rock and Soil Mechanics* 27(6):950-954, DOI: 10.3969/j.issn.1000-7598.2006.06.020 (in Chinese)

Li HZ, Feng J, Song XJ (2014) Research of thrust-sharing in multi-row anti-slide piles. *Journal of Highway and Transportation Research and Development* 31(10):26-31, DOI: 10.3969/j.issn.1002-0268.2014.10.005 (in Chinese)

Li XP, He SM, Luo Y, Wu Y (2011) Numerical studies of the position of piles in slope stabilization. *Geomechanics and Geoengineering* 6(3):209-215, DOI: 10.1080/17486025.2011.578668

Li XP, He SM, Wang CH (2006) Stability analysis of slopes reinforced with piles using limit analysis method. *Geotechnical Special Publication* 9(151):105-112, DOI: 10.1061/40863(195)8

Li XP, He SM, Wu Y (2010) Seismic displacement of slopes reinforced with piles. *Journal of Geotechnical and Geoenvironmental Engineering* 136(6):880-884, DOI: 10.1061/(asce)gt.1943-5606.0000296

Li TB, Liu J, Ren Y, Xue DM, Chen MD (2012a) Sliding mechanism of high-fill slope with pre-reinforced piles at Panzhihua airport. *Journal of Engineering Geology* 20(5):723-731, DOI: 10.3969/j.issn.1004-9665.2012.05.011 (in Chinese)

Li XP, Pei XJ, Gutierrez M, He SM (2012b) Optimal location of piles in slope stabilization by limit analysis. *Acta Geotechnica* 7(3):253-259, DOI: 10.1007/s11440-012-0170-y

Li XP, Su LJ, He SM, Xu J (2016) Limit equilibrium analysis of seismic stability of slopes reinforced with a row of piles. *International Journal for Numerical and Analytical Methods in Geomechanics* 40(8):1241-1250, DOI: 10.1002/nag.2484

Li CD, Tang HM, Hu XL, Wang LQ (2013) Numerical modelling study of the load sharing law of anti-sliding piles based on the soil arching effect for Erliban landslide, China. *KSCE Journal of Civil Engineering* 17(9):1251-1262, DOI: 10.1007/s12205-013-0074-x

Li CD, Wang XY, Tang HM, Lei GP, Yan JF, Zhang YQ (2017) A preliminary study on the location of the stabilizing piles for colluvial landslides with interbedding hard and soft bedrocks. *Engineering Geology* 224:15-28, DOI: 10.1016/j.enggeo.2017.04.020

Li CD, Wu JJ, Tang HM, Wang J, Chen F, Liang DM (2015) A novel optimal plane arrangement of stabilizing piles based on soil arching effect and stability limit for 3D colluvial landslides. *Engineering Geology* 195:236-247, DOI: 10.1016/j.enggeo.2015.06.018

Li CD, Yan JF, Wu JJ, Lei GP, Wang LQ, Zhang YQ (2019) Determination of embedded length of stabilizing piles in colluvial landslides with upper hard and lower weak bedrock based on deformation control principle. *Bulletin of Engineering Geology and the Environment* 78(2):1-20, DOI: 10.1007/s10064-017-1123-3

Li YX, Yang XL (2019) Seismic displacement of 3D slope reinforced by piles with nonlinear failure criterion. *International Journal of Geomechanics* 19(6):04019042, DOI: 10.1061/(ASCE)GM.1943-5622.0001411

Liu B, Su PD, Qiu P, Li ZB (2016) Numerical simulation of the anti-slide pile overtopping of high slope. *Journal of Engineering Geology* 24(s1):940-946, DOI: 10.13544/j.cnki.jeg.2016.s1.136 (in Chinese)

Ma N, Wu HG, Ma HM, Wu XY, Wang GH (2019) Examining dynamic soil pressures and the effectiveness of different pile structures inside reinforced slopes using shaking table tests. *Soil Dynamics and Earthquake Engineering* 116:293-303, DOI: 10.1016/j.soildyn.2018.10.005

Michalowski RL (1995) Slope stability analysis: A kinematical approach. *Géotechnique* 45(2):283-293, DOI: 10.1680/geot.1995.45.2.283

Nian TK, Chen GQ, Luan MT, Yang Q, Zheng DF (2008) Limit analysis of the stability of slopes reinforced with piles against landslides in nonhomogeneous and anisotropic soils. *Canadian Geotechnical Journal* 45(8):1092-1103, DOI: 10.1139/t08-042

Nian TK, Jiang JC, Wang FW, Yang Q, Luan MT (2016) Seismic stability analysis of slope reinforced with a row of piles. *Soil Dynamics & Earthquake Engineering* 84:83-93, DOI: 10.1016/j.soildyn.2016.01.023

Pandit B, Tiwari G, Latha GM, Sivakumar Babu GL (2018) Stability analysis of a large gold mine open-pit slope using advanced probabilistic method. *Rock Mechanics and Rock Engineering* 51(7):2153-2174, DOI: 10.1007/s00603-018-1465-6

Poulos HG (1995) Design of reinforcing piles to increase slope stability. *Canadian Geotechnical Journal* 32(5):808-818, DOI: 10.1139/t95-078

Qin CB, Chian SC, Wang CY (2017) Kinematic analysis of pile behavior for improvement of slope stability in fractured and saturated Hoek - Brown rock masses. *International Journal for Numerical & Analytical Methods in Geomechanics* 41(6):803-827, DOI: 10.1002/nag.2575

Rao PP, Zhao LX, Chen QS, Li L (2017) Limit analysis approach for accessing stability of three-dimensional (3-D) slopes reinforced with piles. *Marine Georesources & Geotechnology* 35(7):978-985, DOI: 10.1080/1064119x.2016.1273982

Sarma SK (1975) Seismic stability of earth dams and embankments. *Géotechnique* 25(4):743-761, DOI: 10.1680/geot.1975.25.4.743

Shan ZL (2002) Stability analysis and reinforcement treatments for the No. 6 Landslide on Shangyu-Sanmen expressway. *The Chinese Journal of Geological Hazard and Control* 13(4):66-72, DOI: 10.3969/j.issn.1003-8035.2002.04.014 (in Chinese)

Shen YJ, Sun HY, Shang YQ, Huang L, Yan KW (2012) Distribution of landslide thrust on cantilever double-row anti-sliding piles. *Chinese Journal of Rock Mechanics and Engineering* 31(S1):2668-2673, DOI: 10.3969/j.issn.1000-6915.2012. z1.010 (in Chinese)

Song YS, Hong WP, Woo KS (2012) Behavior and analysis of stabilizing piles installed in a cut slope during heavy rainfall. *Engineering Geology* 129-130(12):56-67, DOI: 10.1016/j.enggeo.2012.01.012

Sun HY, Zhao Y, Shang YQ, Zhong J (2013) Field measurement and failure forecast during the remediation of a failed cut slope. *Environmental Earth Sciences* 69(7):2179-2187, DOI: 10.1007/s12665-012-2046-8

Tang HM, Hu XL, Xu C, Li CD, Yong R, Wang LQ (2014) A novel approach for determining landslide pushing force based on landslide-pile interactions. *Engineering Geology* 182:15-24, DOI: 10.1016/j.enggeo.2014.07.024

Tang HM, Wasowski J, Juang CH (2019) Geohazards in the Three Gorges Reservoir area, China — Lessons learned from decades of research. *Engineering Geology* 261:105267, DOI: 10.1016/j.enggeo.2019.105267

Wang LP, Zhang G (2013) Pile-reinforcement behavior of cohesive soil slopes: Numerical modeling and centrifuge testing. *Journal of Applied Mathematics* 2013:1-15, DOI: 10.1155/2013/134124

Wang LP, Zhang G (2014) Centrifuge model test study on pile reinforcement behavior of cohesive soil slopes under earthquake conditions. *Landslides* 11(2):213-223, DOI: 10.1007/s10346-013-0388-2

Wei WB, Cheng YM (2009) Strength reduction analysis for slope reinforced with one row of piles. *Computers & Geotechnics* 36(7):1176-1185, DOI: 10.1016/j.compgeo.2009.05.004

Won J, You K, Jeong S, Kim S (2005) Coupled effects in stability

analysis of pile–slope systems. *Computers & Geotechnics* 32(4): 304-315, DOI: 10.1016/j.compgeo.2005.02.006

Wu JJ, Li CD, Liu QT, Fan FS (2017) Optimal isosceles trapezoid cross section of laterally loaded piles based on friction soil arching. *KSCE Journal of Civil Engineering* 21(11):2655-2664, DOI: 10.1007/s12205-017-1311-5

Xiao JH, Gong WP, Martin II JR, Shen MF, Luo Z (2016) Probabilistic seismic stability analysis of slope at a given site in a specified exposure time. *Engineering Geology* 212:53-62, DOI: 10.1016/j.enggeo.2016.08.001

Zhang SL, Zhu ZH, Qi SC, Hu YX, Du Q, Zhou JW (2018) Deformation process and mechanism analyses for a planar sliding in the Mayanpo massive bedding rock slope at the Xiangjiaba Hydropower Station. *Landslides* 15(10):2061-2073, DOI: 10.1007/s10346-018-1041-x

Zheng YR, Chen ZY, Wang GX, Ling TQ (2010) Engineering treatment of slope & landslide, 2nd edition. China Communications Press, Beijing, China, 95-97 (in Chinese)

Appendix

$$f_1=\frac{(3\tan\varphi_l\cos\theta_h+\sin\theta_h)\exp[3(\theta_h-\theta_0)\tan\varphi_l]-3\tan\varphi_l\cos\theta_0-\sin\theta_0}{3(1+9\tan\varphi_l^2)} \tag{20}$$

$$f_2=\frac{1}{6}\frac{L}{r_0}\left(2\cos\theta_0-\frac{L}{r_0}\cos\alpha\right)\sin(\theta_0+\alpha) \tag{21}$$

$$f_3=\frac{\exp[(\theta_h-\theta_0)\tan\varphi_l]}{6}\left[\sin(\theta_h-\theta_0)-\frac{L}{r_0}\sin(\theta_h+\alpha)\right]\times\left\{\cos\theta_0-\frac{L}{r_0}\cos\alpha+\cos\theta_h\exp[(\theta_h-\theta_0)\tan\varphi_l]\right\} \tag{22}$$

$$f_4=\left(\frac{H}{r_0}\right)^2\frac{\sin(\beta-\beta')}{2\sin\beta\sin\beta'}\left[\cos\theta_0-\frac{L}{r_0}\cos\alpha-\frac{H}{3r_0}(\cot\beta+\cot\beta')\right] \tag{23}$$

$$f_5=\frac{(3\tan\varphi_l\sin\theta_h-\cos\theta_h)\exp[3(\theta_h-\theta_0)\tan\varphi_l]-3\tan\varphi_l\sin\theta_0+\cos\theta_0}{3(1+9\tan\varphi_l^2)} \tag{24}$$

$$f_6=\frac{1}{6}\frac{L}{r_0}\left(2\sin\theta_0+\frac{L}{r_0}\sin\alpha\right)\sin(\theta_0+\alpha) \tag{25}$$

$$f_7=\frac{\exp[(\theta_h-\theta_0)\tan\varphi_l]}{6}\left[\sin(\theta_h-\theta_0)-\frac{L}{r_0}\sin(\theta_h+\alpha)\right]\times\left\{\sin\theta_0+\frac{L}{r_0}\sin\alpha+\sin\theta_h\exp[(\theta_h-\theta_0)\tan\varphi_l]\right\} \tag{26}$$

$$f_8=\left(\frac{H}{r_0}\right)^2\frac{\sin(\beta-\beta')}{2\sin\beta\sin\beta'}\left[\sin\theta_0+\frac{L}{r_0}\sin\alpha+\frac{2}{3}\left(\frac{H}{r_0}\right)\right] \tag{27}$$

$$f_9=\frac{1}{2\tan\varphi}\{\exp[2(\theta_h-\theta_0)\tan\varphi_l]-1\} \tag{28}$$

$$\frac{L}{r_0}=\frac{\sin(\theta_h-\theta_0)}{\sin(\theta_h+\alpha)}-\frac{\sin(\theta_h+\beta')}{\sin(\theta_h+\alpha)\sin(\beta'-\alpha)}\left\{\begin{matrix}\sin(\theta_h+\alpha)\exp[(\theta_h-\theta_0)\tan\varphi_l]\\-\sin(\theta_0+\alpha)\end{matrix}\right\} \tag{29}$$

$$\frac{H}{r_0}=\frac{\sin\beta'}{\sin(\beta'-\alpha)}\{\sin(\theta_h+\alpha)\exp[(\theta_h-\theta_0)\tan\varphi_l]-\sin(\theta_0+\alpha)\} \tag{30}$$